This paper is published as part of a *PCCP* themed issue on dynamic nuclear polarization

Guest Editors: Robert Griffin and Thomas Prisner

Editorials

High field dynamic nuclear polarization—the renaissance
R. G. Griffin and T. F. Prisner, *Phys. Chem. Chem. Phys.*, 2010, **12**, 5737
http://dx.doi.org/10.1039/c0cp90019b

The discovery and demonstration of dynamic nuclear polarization—a personal and historical account
Charles P. Slichter, *Phys. Chem. Chem. Phys.*, 2010, **12**, 5741
http://dx.doi.org/10.1039/c003286g

Communications

High power pulsed dynamic nuclear polarisation at 94 GHz
Robert I. Hunter, Paul A. S. Cruickshank, David R. Bolton, Peter C. Riedi and Graham M. Smith, *Phys. Chem. Chem. Phys.*, 2010, **12**, 5752
http://dx.doi.org/10.1039/c002251a

Papers

DNP enhanced NMR using a high-power 94 GHz microwave source: a study of the TEMPOL radical in toluene
Eugeny V. Kryukov, Mark E. Newton, Kevin J. Pike, David R. Bolton, Radoslaw M. Kowalczyk, Andrew P. Howes, Mark E. Smith and Ray Dupree, *Phys. Chem. Chem. Phys.*, 2010, **12**, 5757
http://dx.doi.org/10.1039/c003189e

Rapid sample injection for hyperpolarized NMR spectroscopy
Sean Bowen and Christian Hilty, *Phys. Chem. Chem. Phys.*, 2010, **12**, 5766
http://dx.doi.org/10.1039/c002316g

Slice-selective single scan proton COSY with dynamic nuclear polarisation
Rafal Panek, Josef Granwehr, James Leggett and Walter Köckenberger, *Phys. Chem. Chem. Phys.*, 2010, **12**, 5771
http://dx.doi.org/10.1039/c002710n

Prospects for sub-micron solid state nuclear magnetic resonance imaging with low-temperature dynamic nuclear polarization
Kent R. Thurber and Robert Tycko, *Phys. Chem. Chem. Phys.*, 2010, **12**, 5779
http://dx.doi.org/10.1039/c0cp00157k

Liquid state DNP using a 260 GHz high power gyrotron
Vasyl Denysenkov, Mark J. Prandolini, Marat Gafurov, Deniz Sezer, Burkhard Endeward and Thomas F. Prisner, *Phys. Chem. Chem. Phys.*, 2010, **12**, 5786
http://dx.doi.org/10.1039/c003697h

Exploring the limits of electron-nuclear polarization transfer efficiency in three-spin systems
Nikolas Pomplun and Steffen J. Glaser, *Phys. Chem. Chem. Phys.*, 2010, **12**, 5791
http://dx.doi.org/10.1039/c003751f

Dynamic nuclear polarization experiments at 14.1 T for solid-state NMR
Yoh Matsuki, Hiroki Takahashi, Keisuke Ueda, Toshitaka Idehara, Isamu Ogawa, Mitsuru Toda, Hideo Akutsu and Toshimichi Fujiwara, *Phys. Chem. Chem. Phys.*, 2010, **12**, 5799
http://dx.doi.org/10.1039/c002268c

Trityl biradicals and ^{13}C dynamic nuclear polarization
Sven Macholl, Haukur Jóhannesson and Jan Henrik Ardenkjaer-Larsen, *Phys. Chem. Chem. Phys.*, 2010, **12**, 5804
http://dx.doi.org/10.1039/c002699a

Feasibility of *in vivo* ^{15}N MRS detection of hyperpolarized ^{15}N labeled choline in rats
Cristina Cudalbu, Arnaud Comment, Fiodar Kurdzesau, Ruud B. van Heeswijk, Kai Uffmann, Sami Jannin, Vladimir Denisov, Deniz Kirik and Rolf Gruetter, *Phys. Chem. Chem. Phys.*, 2010, **12**, 5818
http://dx.doi.org/10.1039/c002309b

Polychlorinated trityl radicals for dynamic nuclear polarization: the role of chlorine nuclei
Juan Carlos Paniagua, Verónica Mugnaini, Cristina Gabellieri, Miguel Feliz, Nans Roques, Jaume Veciana and Miquel Pons, *Phys. Chem. Chem. Phys.*, 2010, **12**, 5824
http://dx.doi.org/10.1039/c003291n

Shuttle DNP spectrometer with a two-center magnet
Alexander Krahn, Philip Lottmann, Thorsten Marquardsen, Andreas Tavernier, Maria-Teresa Türke, Marcel Reese, Andrei Leonov, Marina Bennati, Peter Hoefer, Frank Engelke and Christian Griesinger, *Phys. Chem. Chem. Phys.*, 2010, **12**, 5830
http://dx.doi.org/10.1039/c003381b

Properties of dinitroxides for use in dynamic nuclear polarization (DNP)
Cédric Ysacco, Egon Rizzato, Marie-Alice Virolleaud, Hakim Karoui, Antal Rockenbauer, François Le Moigne, Didier Siri, Olivier Ouari, Robert G. Griffin and Paul Tordo, *Phys. Chem. Chem. Phys.*, 2010, **12**, 5841
http://dx.doi.org/10.1039/c002591g

Water ^{1}H relaxation dispersion analysis on a nitroxide radical provides information on the maximal signal enhancement in Overhauser dynamic nuclear polarization experiments

Marina Bennati,[a] Claudio Luchinat,*[b] Giacomo Parigi[b] and Maria-Teresa Türke[a]

Received 2nd February 2010, Accepted 27th April 2010
First published as an Advance Article on the web 10th May 2010
DOI: 10.1039/c002304n

Water ^{1}H relaxation rate measurements of ^{15}N–^{2}H-TEMPONE solutions at temperatures ranging from 298 to 328 K have been performed as a function of magnetic field from 0.00023 to 9.4 T, corresponding to ^{1}H Larmor frequencies of 0.01 to 400 MHz. The relaxation profiles were analyzed according to the full theory for dipolar and contact relaxation, and used to estimate the coupling factor responsible for observed solution DNP effects. The experimental DNP enhancement at ^{1}H Larmor frequency of 15 MHz obtained by saturating one of the lines of the ^{15}N doublet is only *ca.* 20% lower than the limiting value predicted from the relaxation data, indicating that the experimental DNP setup is nearly optimal, the residual discrepancy arising from incomplete saturation of the other line.

Introduction

Dynamic nuclear polarization (DNP) has been shown to be a powerful tool to enhance the sensitivity of NMR experiments through the transfer of the large electron spin polarization to nuclei for almost five decades,[1] and recent studies have shown many attractive applications of this technique.[2–5] The mechanism requires the presence of unpaired electrons in the sample, as contained in radicals or in paramagnetic metal ions. Recently, extensive instrumentation developments have been performed with the aim of applying the DNP mechanism to biological systems in the liquid state, requiring NMR acquisition at high magnetic fields for a good resolution of the macromolecule NMR signals.[6–11] In the liquid state the DNP mechanism is dominated by the Overhauser effect,[1] originating from relaxation processes involving electron and nuclear spins coupled through the hyperfine interaction. Such an effect loses efficiency with increasing field. For this reason it may be convenient to use the DNP mechanism at low fields (*i.e.* around the ^{1}H Larmor frequency of 15 MHz, corresponding to the EPR X-band) and then shuttling the sample into a higher frequency NMR spectrometer.[7,10,12]

The DNP magnetization enhancement due to the Overhauser effect is provided by the ratio between the free electron γ_S and the nuclear γ_I (which amount to 658 for the ^{1}H nucleus) times the product between the saturation factor, the leakage factor and the coupling factor.[1] The saturation factor describes the saturation of the electron Zeeman transitions, the leakage factor the paramagnetic enhancement to the nuclear relaxation rate over the total nuclear relaxation rate, and the coupling factor the magnetization transfer (cross relaxation) from the electron to the nuclear spin when the electron spin is saturated with respect to the capability of the nuclear spin to return to equilibrium once its equilibrium is perturbed through cross relaxation. The limiting factor among the three is the coupling factor, because the saturation and leakage factors can be usually made close to one. Therefore, the coupling factor determines the maximum magnetization enhancement that can be achieved at a fixed magnetic field. It is thus important to correctly evaluate the coupling factor and its dependence on the relevant parameters in order to optimize the experimental conditions for maximum enhancement.

In principle, the coupling factor might be obtained from DNP experiments, however two experimental issues aggravate a proper evaluation of the Overhauser parameters: heating effects due to microwave absorption in water solutions and a complete saturation of the EPR line in particular for radical polarizers with several hyperfine lines. Recently, a lot of attention has been dedicated to the investigation of nitroxide radicals as suited polarizers for DNP in aqueous solution because of their high stability and compatibility with biological samples. Armstrong and Han proposed a method to extrapolate coupling factors of nitroxide radicals from DNP at low microwave power in order to avoid heating effects and to account for the concentration dependence of the saturation factor. Although appealing, this model seemed to underestimate the maximum obtainable DNP enhancement and consequently the coupling factor.[13–15]

Hausser and Stehlik[1] proposed already in the 70s that an independent way to estimate the coupling factor is based on the measurement of the field dependence of the nuclear longitudinal relaxation rates. Relaxometry can provide the ^{1}H relaxation rates from very low magnetic field (*i.e.*, 0.00023 T, corresponding to a ^{1}H Larmor frequency of 0.01 MHz) up to 1 T,[16–19] and additional data at higher fields can be obtained using conventional NMR spectrometers. The method has been applied later on by Wind and Ardenkjaer-Larsen to rationalize

[a] *Max Planck Institute for Biophysical Chemistry, Göttingen, Germany*
[b] *Magnetic Resonance Center (CERM), University of Florence, Via Luigi Sacconi 6, 50019 Sesto Fiorentino, Italy. E-mail: luchinat@cerm.unifi.it*

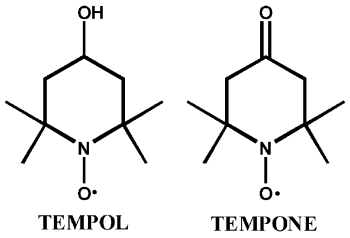

Scheme 1

the DNP enhancements observed with trityl radicals in water solution;[20] they obtained best agreement between the coupling factor from NMR data and from DNP experiments. We have recently applied the same method to evaluate the coupling factor of nitroxide radical and reported a value for ^{14}N-TEMPOL at ^{1}H Larmor frequencies of 15 and 140 MHz.[7]

In this paper we present the relaxation rate profiles of ^{15}N–^{2}H-TEMPONE (see Scheme 1) solutions at different temperatures, the nitroxide radical for which we could report the highest DNP enhancements measured at ^{1}H Larmor frequencies of 15 (X-band) and 140 MHz (W-band). The acquired Nuclear Magnetic Relaxation Dispersion (NMRD) data have been analyzed according to the full relaxation theory to obtain estimates of the parameters governing the relaxation rates and to calculate the coupling factor of the radical as a function of temperature. The results are discussed in the light of the observed DNP enhancements.

Theoretical background

For a system with a nucleus I subject to hyperfine coupling with an electron S, the rate of variation with time of the nuclear magnetization along the magnetic field direction, M_z^{I}, after a perturbation from its equilibrium value, $M_z^{\mathrm{I}}(\infty)$, depends on the transition probabilities among the different proton–electron spin levels (see Fig. 1) and on the relaxation processes not involving the electron spin, $R_{1\mathrm{dia}}$, as described by eqn (1)

$$\frac{\mathrm{d}M_z^{\mathrm{I}}(t)}{\mathrm{d}t} = -(w_0 + 2w_1^{\mathrm{I}} + w_2 + R_{1\mathrm{dia}})(M_z^{\mathrm{I}}(t) - M_z^{\mathrm{I}}(\infty)) - (w_2 - w_0)(M_z^{\mathrm{S}}(t) - M_z^{\mathrm{S}}(\infty)) \quad (1)$$

where M_z^{S} is the electron magnetization along the z direction. At the steady state $\left(\frac{\mathrm{d}M_z^{\mathrm{I}}(t)}{\mathrm{d}t} = 0\right)$ DNP conditions, the magnetization $M_{z(\mathrm{ss})}^{\mathrm{I}}$ becomes

$$M_{z(\mathrm{ss})}^{\mathrm{I}} = M_z^{\mathrm{I}}(\infty) - \frac{w_2 - w_0}{w_0 + 2w_1^{\mathrm{I}} + w_2 + R_{1\mathrm{dia}}}(M_{z(\mathrm{ss})}^{\mathrm{S}} - M_z^{\mathrm{S}}(\infty)) \quad (2)$$

and thus

$$\frac{M_{z(\mathrm{ss})}^{\mathrm{I}}}{M_z^{\mathrm{I}}(\infty)} = 1 + \frac{w_2 - w_0}{w_0 + 2w_1^{\mathrm{I}} + w_2}\frac{w_0 + 2w_1^{\mathrm{I}} + w_2}{w_0 + 2w_1^{\mathrm{I}} + w_2 + R_{1\mathrm{dia}}} \times \frac{M_z^{\mathrm{S}}(\infty) - M_{z(\mathrm{ss})}^{\mathrm{S}}}{M_z^{\mathrm{S}}(\infty)}\frac{M_z^{\mathrm{S}}(\infty)}{M_z^{\mathrm{I}}(\infty)} = 1 - \xi f s\left|\frac{\gamma_{\mathrm{S}}}{\gamma_{\mathrm{I}}}\right| \quad (3)$$

where the three fractions represent the coupling factor ξ, the leakage factor f and the saturation factor s, respectively. The paramagnetic enhancement to the nuclear relaxation rate, $R_{1\mathrm{para}}$, is actually provided by

$$R_{1\mathrm{para}} = w_0 + 2w_1^{\mathrm{I}} + w_2 \quad (4)$$

and the total nuclear relaxation rate is given by the sum of the paramagnetic and the diamagnetic contributions,

$$R_1 = R_{1\mathrm{para}} + R_{1\mathrm{dia}}. \quad (5)$$

As a result, the leakage factor represents the ratio between $R_{1\mathrm{para}}$ and R_1 and approaches 1 when the diamagnetic contribution to the relaxation rate is negligible with respect to the paramagnetic contribution. Since $R_{1\mathrm{para}}$ increases linearly (see later) with the concentration of the paramagnetic species in solution, the leakage factor also increases up to the maximum value of 1 when the concentration of the paramagnetic molecule increases. The direct measurement of the nuclear longitudinal relaxation rate of the investigated sample in the presence and in the absence of the paramagnetic species in solution thus provides a direct and safe estimate of the leakage factor.

From the perturbing time-dependent Hamiltonian relative to the hyperfine coupling between nuclear and electron spins the following transition probabilities between the different spin levels originating in the presence of a magnetic field can be calculated[21,22]

$$w_0 = kJ(\omega_{\mathrm{I}} - \omega_{\mathrm{S}},\tau_{\mathrm{c}}) + k_{\mathrm{a}}J(\omega_{\mathrm{I}} - \omega_{\mathrm{S}},\tau_{\mathrm{a}}) \quad (6)$$

$$w_1^{\mathrm{I}} = \tfrac{3}{2}kJ(\omega_{\mathrm{I}},\tau_{\mathrm{c}})$$

$$w_2 = 6kJ(\omega_{\mathrm{I}} + \omega_{S},\tau_{\mathrm{c}})$$

where $J(\omega,\tau)$ is the Lorentzian spectral density function

$$J(\omega,\tau) = \frac{\tau}{1 + \omega^2\tau^2},$$

τ_{c} is the correlation time for the dipolar interaction and τ_{a} is the correlation time for the contact interaction. The dipolar interaction is modulated by fluctuations due to molecular reorientation, electron relaxation and exchange of the interacting nucleus, so that its correlation time is determined by the reorientation time of the molecule bearing the paramagnetic electron, τ_{R}, the electron relation time, τ_{s}, and the nucleus lifetime, τ_{M}; the contact

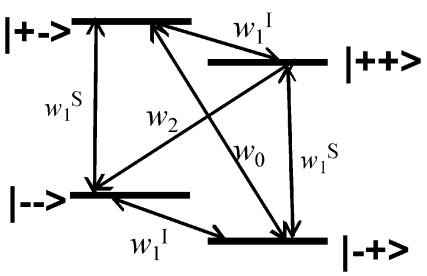

Fig. 1 Energy levels and transition probabilities in a magnetically coupled electron-nuclear spin system.

interaction has a correlation time determined by τ_s and τ_M only, so that

$$\tau_c = (\tau_R^{-1} + \tau_s^{-1} + \tau_M^{-1})^{-1} \quad (7)$$

$$\tau_a = (\tau_s^{-1} + \tau_M^{-1})^{-1}.$$

If the nucleus I belongs to a ligand able to exchange between a position where it is bound to the paramagnetic molecule and a position where it is free in solution, in case of a fast exchanging regime (*i.e.*, τ_M^{-1} larger than the relaxation rate of the nucleus in the bound position) the detected NMR signal is the weighted average between that of the nucleus in the free ligand and in the bound position. In the presence of a large amount of ligand with respect to the paramagnetic molecule concentration, the signal shift and relaxation parameters are close to those of the free ligand but still contain information on the species bound to the paramagnetic center. Accordingly, the constants k and k_a are

$$k = f_M \frac{2}{15}\left(\frac{\mu_0}{4\pi}\right)^2 \frac{\gamma_I^2 g_e^2 \mu_B^2 S(S+1)}{r^6}$$

$$k_a = f_M \frac{2}{3} S(S+1)\left(\frac{A}{\hbar}\right)^2$$

where r is the distance between nucleus and electron spins in the bound positions, A is the contact coupling constant, and f_M is the mole fraction of ligand nuclei in bound positions.

The hyperfine interaction can be conveniently split into dipolar and contact terms, the former depending on the distance, r, between the electron and nuclear spins, the latter on the contact coupling constant, A. The overall paramagnetic enhancement to the relaxation rate can thus be written as the sum of a dipolar and a contact contribution. Assuming that the nuclear Larmor frequency is negligible with respect to the electron Larmor frequency, this yields

$$R_{1para} = R_{1dip} + R_{1cont} \quad (8)$$

$$R_{1dip} = k(7J(\omega_S,\tau_c) + 3J(\omega_I,\tau_c))$$

$$R_{1cont} = k_a J(\omega_S,\tau_a).$$

As a result, the dipolar contribution to the relaxation rate has a value of 10 $k\tau_c$ at very low magnetic fields, and then for increasing fields, the profile shows: (i) a Lorentzian dispersion centered at frequency $\tau_c/(2\pi|\gamma_S/\gamma_I|)$ (corresponding to $\omega_S\tau_c = 1$); (ii) a plateau value of 3 $k\tau_c$; and (iii) a further dispersion at frequency $\tau_c/(2\pi)$ (corresponding to $\omega_I\tau_c = 1$), down to zero (see Fig. 2A). The contact contribution to the relaxation rate has only one dispersion centered at frequency $\tau_a/(2\pi|\gamma_S/\gamma_I|)$, down to zero (Fig. 2B). It was suggested[1] that a further term should be considered in R_{1cont} proportional to $J(\omega_I,\tau_a)$, with a weighting factor β. Such term is ascribed to the nuclear relaxation transitions induced by electronic relaxation transitions as a consequence of the hyperfine perturbation of the Zeeman states due to the scalar coupling. This term is predicted to be negligible when the electron relaxation time τ_s is much larger than the nucleus lifetime τ_M as is common for radicals. Therefore, this term should be negligible in our case.

Finally, the coupling factor results

$$\xi = \frac{5kJ(\omega_S,\tau_c) - R_{1cont}}{R_{1para}} \quad (9)$$

which can be rearranged in the following form

$$\xi = \frac{5}{7}\left[1 - \frac{3kJ(\omega_I,\tau_c)}{R_{1para}}\right] - \frac{12}{7}\frac{R_{1cont}}{R_{1para}}. \quad (10)$$

Eqn (10) shows that for a purely dipolar interaction the coupling factor can have any value between 0 (for $R_{1dip} = 3kJ(\omega_I,\tau_c)$) and 0.5 (for $R_{1dip} = 10k\tau_c$), and for a purely contact interaction ξ is always -1. Fig. 3 shows the values of ξ as a function of the magnetic field for different ratios of the low field contact and dipolar contributions. As already pointed out,[23] when contact relaxation is dominant very large DNP enhancements may result even at high magnetic fields. On the contrary, small contact contributions are predicted to reduce the absolute value of the coupling factor.

The constant k reported above has been calculated assuming that the nucleus has a fixed distance r from the electron for the lifetime τ_M, and the rest of the time in the bulk solution at a distance from the metal which may be considered infinite. The time spent in approaching and leaving the binding site has thus been considered negligible. Contributions from nuclei not bound to the paramagnetic molecule and diffusing around it can also be evaluated as described for instance in the outer-sphere model developed by Freed.[24] Other models have been proposed over the years, all providing, with different parameters, an overall agreement with the Freed model.[25–27] When such contributions cannot be neglected they must be added to the inner-sphere relaxation arising from nuclei coordinated in fixed positions to the paramagnetic molecule. This happens when the distance of closest approach is similar to the distance of the bound nuclei and the correlation time τ_c is of the same order or smaller than the diffusional correlation time. The latter depends on the size of both the nucleus-bearing molecule and the paramagnetic molecule, according to their diffusion coefficients D_L and D_M, respectively, and of the distance of closest approach d between nucleus and electron spins

$$\tau_D = \frac{d^2}{D_M + D_L}. \quad (11)$$

Assuming that the distance of closest approach is the same for all directions from which the nucleus is approaching the paramagnetic molecule (*i.e.* the unpaired electron is at the center of a spherical molecule) and that the electron relaxation time is much longer than the diffusional time, the diffusional Freed model indicates that the additional outer-sphere contribution to the nuclear relaxation can be calculated using the same expressions for the transition probabilities already used for the inner-sphere dipolar interaction with a coordinated nucleus, *i.e.*,

$$w_0 = k'\tilde{J}(\omega_I - \omega_S,\tau_D) \quad (12)$$

$$w_1^I = \tfrac{3}{2}k'\tilde{J}(\omega_I, \tau_D)$$

$$w_2 = 6k'\tilde{J}(\omega_I + \omega_S,\tau_D)$$

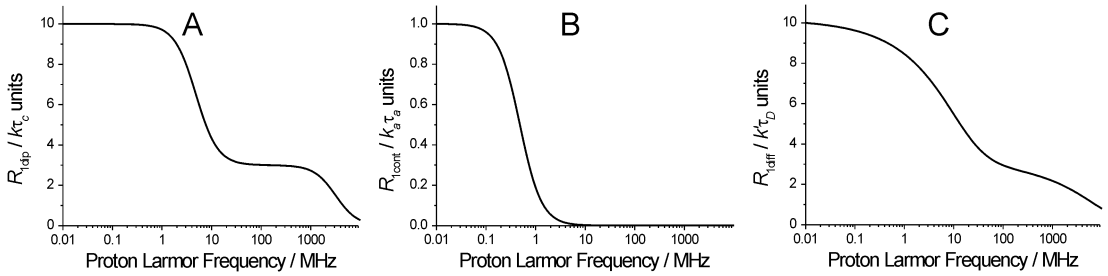

Fig. 2 Paramagnetic enhancement to the nuclear relaxation rate as a function of the applied magnetic field: (A) inner-sphere dipolar contribution; (B) contact contribution; and (C) outer-sphere contribution. The profiles are calculated for a correlation/diffusional time of 50 ps.

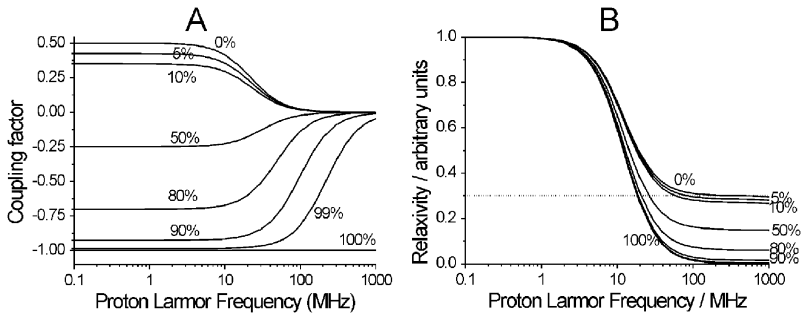

Fig. 3 (A) Field dependence of the coupling factor for different ratios of the low field contact contribution to the ^{1}H relaxation rate with respect to the total (inner-sphere dipolar plus contact) relaxation rate. The field dependence of the latter is shown in B. All calculations are performed for correlation times of 20 ps.

with

$$k' = \frac{32000\pi}{405}\left(\frac{\mu_0}{4\pi}\right)^2 \frac{N_A[M]\gamma_I^2 g_e^2 \mu_B^2 S(S+1)}{d(D_M + D_L)},$$

$$\tilde{J}(\omega,\tau) = \frac{1 + 5z/8 + z^2/8}{1 + z + z^2/2 + z^3/6 + 4z^4/81 + z^5/81 + z^6/648},$$

$z = (2\omega\tau_D)^{0.5}$ and $[M]$ representing the molar concentration of the paramagnetic moiety (expressed in mol dm^{-3}). In the more realistic case of the unpaired electron not being at the center of a spherical molecule, the distance d represents a weighted average of the real distances.

The overall nuclear longitudinal relaxation enhancement is thus the sum of the following contributions:

$$R_{1para} = R_{1dip} + R_{1cont} + R_{1diff} \quad (13)$$

where

$$R_{1diff} = k'(7\tilde{J}(\omega_S,\tau_D) + 3\tilde{J}(\omega_I,\tau_D)) \quad (14)$$

(see Fig. 2C) and the coupling factor results

$$\xi = \frac{5}{7}\left[1 - \frac{3kJ(\omega_I,\tau_c) + 3k'\tilde{J}(\omega_I,\tau_D)}{R_{1para}}\right] - \frac{12}{7}\frac{R_{1cont}}{R_{1para}}. \quad (15)$$

Fig. 2C shows that the outer-sphere relaxation profile has the same features than the dipolar inner-sphere relaxation profile, all dispersions being however much more stretched.

Results and discussion

Coupling factor of ^{15}N–^{2}H-TEMPONE at the ^{1}H Larmor frequency of 15 MHz

The relaxation profiles of solvent water ^{1}H nuclei in the presence of TEMPONE 10 mM and 25 mM at 298 K have been measured with a fast field cycling relaxometer[28,29] and reported in Fig. 4 together with the relaxation profile of pure water protons. Errors are estimated to be less than 1%. A measurement at ^{1}H Larmor frequency of 400 MHz was also performed using a Bruker spectrometer for the sample with the lower radical concentration. The paramagnetic enhancements to the relaxation rates were then obtained after subtraction of the diamagnetic contribution corresponding to the pure water ^{1}H relaxation rates and divided by the radical concentration, to obtain the ^{1}H relaxivity (Fig. 5). As expected, the latter was the same within the error for the two samples at different concentrations, in agreement with a linear dependence of the paramagnetic relaxation enhancement on the concentration of the paramagnetic species.

In order to calculate the coupling factor at ^{1}H Larmor frequency of 15 MHz we can first suppose that the contact contribution to the relaxation rate is negligible, as always done for nitroxide radicals.[25,27,30] The relaxation profile shows that at 15 MHz the first dispersion is occurring; the dispersion corresponding to $\omega_I\tau_c = 1$ can be thought not to have started yet. This means that the term $3kJ(\omega_I,\tau_c) + 3k'\tilde{J}(\omega_I,\tau_D)$ in eqn (15) has a value equal to 3/10 of the low field R_{1para} value, which is 4.79 s^{-1} at 10 mM. Since at the same concentration $R_{1para} = 2.84$ s^{-1}, the coupling factor at 15 MHz is

$$\xi = \frac{5}{7}\left(1 - \frac{\frac{3}{10}(4.79 \pm 0.04)}{2.84 \pm 0.04}\right) = 0.35 \pm 0.02$$

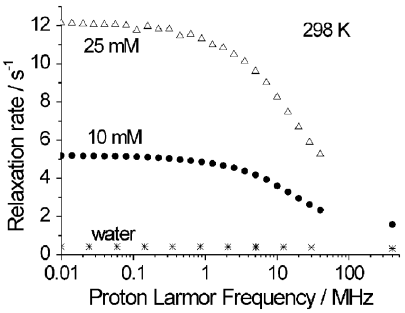

Fig. 4 Solvent water ^{1}H relaxation profiles for solutions of TEMPONE 10 mM and 25 mM at 298 K.

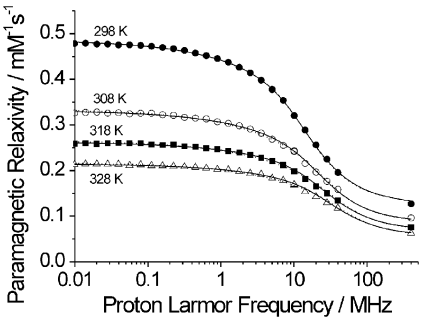

Fig. 6 Best fit of the normalized paramagnetic nuclear relaxation rates at 298, 308, 318 and 328 K. The profiles calculated with leaving the D parameter free to change in the fitting procedure or fixed to the expected values are shown as solid lines and dotted lines, respectively.

independently of the concentration of the radical in solution. Errors are given by the instrumental precision in measuring the rates of the radical solution and of pure water. It is to be noted that such an estimated value of the coupling factor has been calculated from the measured relaxation rates using only the assumptions that: (i) the contact relaxation is negligible; and (ii) the $3kJ(\omega_I,\tau_c) + 3k'\tilde{J}(\omega_I,\tau_D)$ term at 15 MHz can be estimated from the low field value. The value is in good agreement with the value we obtained in Höfer *et al.*[7] for the radical ^{14}N-TEMPOL and the value obtained by Armstrong and Han,[14] using the same technique.

Relaxation rate measurements were also performed at 308, 318 and 328 K (Fig. 6) in order to monitor the increase in the coupling factor expected with increasing temperature. This is in fact a result of the decrease of the correlation time τ_c and of the diffusional time, corresponding to the increase in the diffusion coefficients with temperature. The coupling factors resulting from the experimental relaxation rates at ^{1}H Larmor frequency of 15 MHz with respect to the low field values were 0.39, 0.41 and 0.43 at 308, 318 and 328 K, respectively.

An accurate fit of the relaxation profiles was then performed in order to check the correctness of the assumptions and to obtain the parameters responsible for water ^{1}H relaxation.

Selection of the model for the relaxation mechanisms from the relaxation profiles

The possible presence of a non-negligible contact contribution to the paramagnetic relaxation rate can be monitored by checking the ratio between high field and low field relaxivity. In fact, in the absence of a contact contribution the relaxation rate after the observed ω_S dispersion (and before the ω_I dispersion) should amount to 3/10 of the low field relaxation rate, whereas in the presence of a contact contribution it should be smaller (Fig. 3B). Fig. 5A shows that the relaxivity at ^{1}H Larmor frequency of 400 MHz and 298 K is slightly smaller than 3/10 of the low field relaxivity. However, it should be noted that the ω_S and ω_I dispersions are not well separated in the case of the outer-sphere relaxation, differently from the inner-sphere case, as clearly shown in Fig. 2. Such a small reduction could thus be ascribed to the ω_I dispersion, which may thus have already started at 400 MHz.

The profile was thus fit using the outer-sphere model eqn (14), and the fit, reported in Fig. 5A as solid line, was rather good, although not perfectly satisfactory. The best fit parameters available from the fit were the distance of closest approach $d = 2.4$ Å and the diffusion coefficient $D = D_L + D_M = 2.4 \times 10^{-9}$ m^2 s^{-1}. The latter value seems actually too small, as it corresponds to the diffusion coefficient of free water (D_L) at 298 K alone. The diffusion coefficient of TEMPONE at the same temperature can be estimated to be about 0.4×10^{-9} m^2 s^{-1}, as recently reported in Armstrong & Han.[14] In any case, the coupling factor obtained from the best-fit parameters is 0.36. The non-perfect agreement between the best-fit profile and the experimental data, and the too-small value obtained for the diffusion coefficient, however, prompted us to analyse the data using different models.

If the same profile is fit using the inner-sphere model eqn (8), a very bad fit to the dispersion is obtained (dotted line in

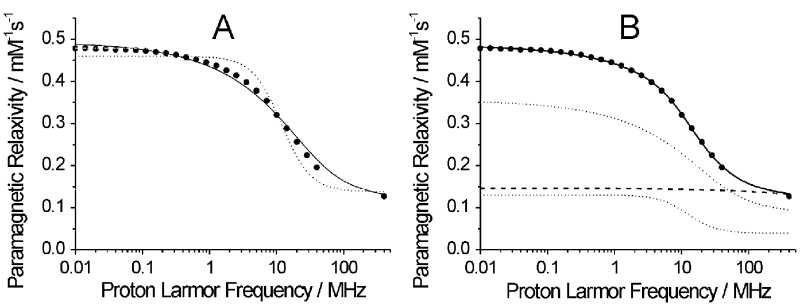

Fig. 5 (A) Best fit of the normalized paramagnetic nuclear relaxation rates using the outer-sphere model (solid line) or the inner-sphere model (dotted line). (B) Best fit of the normalized paramagnetic nuclear relaxation rates using both outer-sphere and inner-sphere contributions (solid line). The individual contributions are also reported as dotted lines (upper and lower dotted curves, respectively). The ω_I terms are shown as dashed line.

Fig. 5A), so that such model can be excluded. A very good fit of the profile is actually obtained when both inner-sphere and outer-sphere models are used (eqn (13)), even in the case of no contact contributions (solid line in Fig. 5B). The contributions of outer-sphere and inner-sphere relaxivity are indicated as dotted lines, the latter amounting to about 25% of the total at low fields. The sum of the corresponding ω_I spectral density functions is also shown as dashed line. It may be appreciated that it remains basically constant up to 100 MHz and starts decreasing slightly at higher frequencies, so that a good fit could be obtained even without considering the presence of the contact term.

Best-fit analysis of the relaxation profiles of TEMPONE

The relaxivity profiles acquired at the four temperatures were thus fit simultaneously using a unique value of d and r. The resulting best fit parameters are reported in Table 1 and the profiles are shown in Fig. 6 as solid lines. The coupling factors at 15 MHz calculated from the above parameters and eqn (15) are also reported in Table 1. In this case, the value of D at 298 K corresponds to the expected value. The diffusional time τ_D calculated from the d and D values at 298 K is 26 ps. It is quite similar to the correlation time modulating the inner-sphere dipolar relaxation, τ_c. The electron relaxation rate in nitroxides has been estimated to be of the order of 10^{-7} s.[25] Therefore, τ_c must be determined by either the reorientation time of TEMPONE, τ_R, or the lifetime τ_M of two coordinated water protons, located at a distance of about 3.0 Å, or of one water proton at 2.6 Å, whichever is shorter. The best fit values obtained for D are somewhat larger than expected from experimental measurements of water diffusion[31] or than expected from the temperature dependence of water viscosity (η), according to the law

$$D = \frac{kT}{6\pi a\eta} = D_{298\ \mathrm{K}}\frac{T}{\eta}\frac{\eta_{298\ \mathrm{K}}}{298}$$

with the diffusion coefficient at 298 K set to 2.87×10^{-9} m^2 s^{-1}. The τ_c values decrease with temperature as expected from the Stokes' law, and similarly with the diffusional time.

The fits were also performed by fixing the diffusion coefficient to the expected values of 3.7, 4.6 and 5.6×10^{-9} m^2 s^{-1} at 308, 318 and 328 K, respectively. The fit profiles are slightly worse (see dotted lines in Fig. 6), with best fit τ_c values of 8.9, 6.8 and 5.6 ps at 308, 318 and 328 K, respectively.

Using the best-fit parameters of Table 1 the coupling factor was also calculated at 140 MHz, and resulted in 0.05, 0.09, 0.11 and 0.14 at 298, 308, 318 and 328 K, respectively, independently of whether the fit is performed with fixed or free D parameters. An error for the coupling factor of ±0.03 is estimated from the standard deviation of the best fit parameters, but it may be larger depending on the accuracy of the modeled dispersions of the spectral density functions (see later).

The distance of closest approach (2.7 Å) is somewhat larger than expected for the distance between the unpaired electron (delocalized between the nitrogen and oxygen positions) and the water proton in a hydrogen-bound position. However, it should be noted that the unpaired electron is not located at the center of a spherical molecule, but rather close to one border of a flat surface. The actual distance of closest approach is thus different depending on the direction from which water molecules approach the nitroxide, and the value which is obtained represents a weighted average. A value for d of 2.7 Å seems to represent a better average among the real distances of closest approach of water protons from the unpaired electron than the previously proposed values of 4–5 Å.[14] In fact water protons approaching the nitroxide along the O–N direction can be at distances as short as 1.9 Å from the oxygen,[30] and quantum mechanical calculations indicated that the electron density of the unpaired electron is located almost 50% at the oxygen atom and 50% at the nitrogen atom.[32–34] As already pointed out in Polnaszek & Bryant,[25] using the outer-sphere model in cases where the unpaired electron is not located at the center of a spherical molecule results: (i) in d values shorter than those expected from the distance between intermolecular centers; and (ii) in a D value representing an upper bound limit of the correct diffusion coefficient value. Therefore, in cases of an off-center position for the unpaired electron, as the present system, the real diffusion coefficient will be smaller than the best-fit D value (and larger than that of pure water), as also experimentally found.

The relaxation profiles can thus be nicely fit with the sum of outer-sphere and inner-sphere contributions. The outer-sphere contribution describes the long-time decay of the autocorrelation function which, due to the character of the translational Brownian dynamics, has a time dependence described by $(Dt)^{-3/2}$ independently of the assumed model. It thus arises from modulations of the water proton–electron dipolar interactions at large intermolecular distances. The picture becomes more complicated when water molecules move around the radical, down to a distance of closest approach. Due to the off-center position of the unpaired electron within the non spherical nitroxide molecule, different distances of closest approach should be considered depending on the direction along which the water molecules approach the TEMPONE radical. Therefore, the obtained value for the distance of closest approach is a kind of average resulting from the different contributions coming from water molecules with quite different collision distances between protons and unpaired electron. On the other hand, the autocorrelation functions

Table 1 Best fit values of the parameters (d, D, τ_c and r) obtained from the relaxation dispersion profiles and resulting values for τ_D and ξ

Temperature/K	d/Å	D/m^2 s^{-1}	τ_D/s	τ_c/s	r/Å[a]	ξ (at 15 MHz)
298	2.72 ± 0.05	(2.87 ± 0.05) × 10^{-9}	26 × 10^{-12}	(20 ± 1) × 10^{-12}	2.96 ± 0.05	0.35
308		(4.15 ± 0.09) × 10^{-9}	18 × 10^{-12}	(13 ± 1) × 10^{-12}		0.39
318		(5.47 ± 0.14) × 10^{-9}	14 × 10^{-12}	(11 ± 1) × 10^{-12}		0.41
328		(6.88 ± 0.23) × 10^{-9}	11 × 10^{-12}	(10 ± 1) × 10^{-12}		0.43

The error corresponds to the standard deviation.[a] Assuming two protons.

corresponding to the dipolar interactions around the unpaired electron position are well described by exponential decays. They take into account fluctuations in the dipole–dipole interaction energy arising from either rotations of the nitroxide molecule, with an off-center unpaired electron,[20] and rotations of the complex of the solvent molecules with the radicals. The latter term is actually effective only if the complex lifetime is longer than the reorientation time of the system. This should not be the case of TEMPONE, as indicated by molecular dynamics calculations.[15,30] Therefore, the inner-sphere contribution must be accounted for, together with the outer-sphere contribution, by a correlation time of the same order of d^2/D, or of the nitroxide reorientation time. The diffusional correlation time and the radical reorientation time are in fact both related to the hydrodynamic mobilities of solvent and radical, and result in the same order of magnitude.[35,36]

Finally, the fit was performed by including a contact contribution. The fit was slightly better, as expected due to the increased number of fitting parameters. The values of the best fit parameters changed modestly (the correlation time within 30%, $r = 3.26 \pm 0.6$ Å and $d = 2.53 \pm 0.3$ Å), and a value for A/h of 1.4 ± 0.2 MHz was found. The latter value may be consistent with computational estimations[30] and typical values obtained for different systems.[19] In principle, an additional correlation time for contact relaxation should be included in the fitting procedure, but the experimental data are not sensitive enough to provide reliable best-fit values of so many parameters. The coupling factors calculated from the best fit parameters are reported in Table 2.

Comparison of the calculated coupling factors with the experimentally available DNP signal enhancements

The coupling factors obtained for ^{15}N–^{2}H-TEMPONE can be used to estimate the maximal enhancements achievable in a DNP experiment under the ideal condition of a saturation factor equal to unity. The coupling factors calculated with or without a possible contact contribution at the different temperatures and two frequencies are reported in Table 2 together with the leakage factors, extracted from the present relaxation dispersion data. The corresponding maximal DNP enhancements calculated using eqn (3) are also reported.

If contact contributions to relaxation are considered negligible, the NMRD data lead to a maximal enhancement of −218 at 298 K and 15 MHz, which is somewhat higher than the experimental value of −170 at the same temperature 298 K and 15 MHz (see companion paper, Türke *et al.*[39]). Table 3 shows a comparison between the experimental DNP enhancement measured for different radical concentrations (Türke *et al.*) with the enhancement predicted by NMRD data from the best fit parameters obtained with considering contact contributions. Due to the different irradiation time needed for saturating the different samples, the resulting temperatures were different, and therefore different values for the coupling factors have been considered for the different samples together with the corresponding NMRD derived leakage factors. The ratio between the experimental DNP enhancement and the NMRD derived maximum enhancement, calculated assuming $s = 1$, is broadly constant for all samples, *ca.* 0.8. This confirms the extent of the reduction in the measured enhancement, which is thus independent on the radical concentration (at least in the investigated range).

The agreement in the order of magnitude of the observed DNP enhancements with the predicted maximal enhancements indicates that the optimization of the DNP set up at 15 MHz has allowed us to reach enhancements close to the theoretical limit.

The remaining discrepancy of about 20% could arise from different factors. The presence of a modest contribution from contact relaxation cannot be ruled out. However, from the NMRD data this contribution can be hardly responsible for more than about 5% reduction of the coupling factor at 15 MHz (see Table 2). Another possible origin for the discrepancy could be that the ideal condition of full saturation might not be fulfilled during the DNP experiments. It was found that increasing the power of the microwave used to saturate one of the two EPR transitions from 4 to 30 W, the enhancement remained constant (Türke *et al.*), thus indicating that such transition has been completely saturated. However, this by itself does not ensure that both EPR transitions are completely saturated. The difficulty of saturating the two hyperfine lines of ^{15}N–^{2}H-TEMPONE EPR spectrum has been discussed extensively in the recent literature[14,37,38] and might not be overcome entirely in an experimental set up with one frequency irradiation. ELDOR measurements (Türke *et al.*) actually indicate that the saturation factor for the non irradiated transition amounts to about 0.6. The overall saturation factor in eqn (3) should thus be the average between the saturation factor of the irradiated and the non irradiated transitions, which are 1 and 0.6, respectively. Therefore, an s value equal to 0.8 is obtained (Türke *et al.*), in perfect agreement with the s value estimated here from the coupling factor obtained by NMRD.

The spectral densities used in the present paper to fit the NMRD data are based on the force free model, which still

Table 2 Maximum DNP enhancement predicted from the analysis of the relaxation data

^{1}H Larmor frequency/MHz	Temp./K	ξ_{NMRD} [a]	f_{NMRD} (25 mM)	ε_{max} ($s = 1$) [a]	ε_{DNP}
15	298	0.35/0.33	0.95	−218/−205	−170
	308	0.39/0.36	0.95	−243/−222	
	318	0.41/0.37	0.95	−255/−228	
	328	0.43/0.37	0.95	−268/−232	
140	298	0.05/0.07	0.91	−29/−41	
	308	0.09/0.11	0.91	−53/−65	−43
	318	0.11/0.14	0.91	−65/−83	
	328	0.14/0.16	0.91	−83/−95	

[a] The two values are calculated without and with inclusion of a contact contribution in the fit of the relaxation profiles, respectively.

Table 3 Comparison of the experimental DNP enhancement with the enhancement predicted by NMRD data

Conc./mM	T/K	f_{NMRD}	ξ_{NMRD}	ε_{max} (s = 1)	ε_{DNP}	s = $\varepsilon_{DNP}/\varepsilon_{max}$
5	313	0.78	0.365	−186	−148	0.79
10	309	0.88	0.36	−207	−160	0.77
25	300	0.95	0.335	−208	−170	0.82
50	297	0.97	0.33	−210	−165	0.79

represents an approximation of the atomistic phenomena. Although the data fits are very satisfactory, the model could lead to some uncertainties in the values of the best fit parameters that are difficult to quantify. In a recent paper,[30] Sezer *et al.* calculated spectral density functions for DNP with TEMPOL using MD simulations and arrived at a coupling factor of 0.3 at 15 MHz (for room temperature), which is somewhat lower than the one we obtained from our NMRD analysis (0.35). The direct determination of the spectral density function from very low fields up to the ^{1}H Larmor frequency of 40 MHz, however, allows us to directly estimate the value of the coupling factor up to such a frequency, independently of the accuracy of the model, in the assumption that: (i) relaxation is driven by the modulation of the dipolar interaction between protons and unpaired electron (as assumed also in the MD simulations); and (ii) the dispersions of the spectral density functions $J(\omega_I,\tau_c)$ and $\tilde{J}(\omega_I,\tau_D)$ have not yet started at such frequencies. The validity of the first assumption is confirmed by the data acquired at 400 MHz; the validity of the second assumption by the shape of the observed relaxation profiles. In fact, the $J(\omega_I,\tau_c)$ and $\tilde{J}(\omega_I,\tau_D)$ terms must have the same field dependence of the $J(\omega_S,\tau_c)$ and $\tilde{J}(\omega_S,\tau_D)$ terms, being only translated in frequency of a $|\gamma_S/\gamma_I|$ factor. Inaccuracies in the coupling factor due to approximations in the force free model can thus arise only at ^{1}H Larmor frequencies larger than 40 MHz, for which the dispersions of the spectral density functions $J(\omega_I,\tau_c)$ and $\tilde{J}(\omega_I,\tau_D)$ start occurring and the direct measurement of the relaxation rate was not possible but the corresponding value could only be interpolated from the available data and the interaction model.

A comparison between DNP experiments and NMRD data at 140 MHz/95GHz is less straightforward as the sample temperature could not be measured with accuracy at this frequency. However, there is a great interest in exploring the capability of 140 MHz/95 GHz solution DNP so that a short discussion is noteworthy. So far we have measured a DNP enhancement at 140 MHz of –43. The NMRD coupling factor at 140 MHz and room temperature (Table 2) predicts a maximal enhancement that would be consistent with the DNP experimental value. However, due to the very tiny size of the W-band sample tubes (0.1 mm inner diameter) the heating effects could be considerable depending on the experimental conditions. The temperature in the sample during the DNP measurements was actually estimated by measuring the reduction of the cavity quality factor, and the shift yielded an increase of about 15 K (Türke *et al.*). Our present NMRD results indicate that the coupling factor doubles for a temperature raise of only 10–20 K, which suggests that much larger DNP enhancements might be observable in the future.

Acknowledgements

Malini Nagulapalli is acknowledged for the help in the measurement of the relaxation rates at ^{1}H Larmor frequency of 400 MHz. This work was supported by Ente Cassa di Risparmio di Firenze, by the Max Planck Society and by the European Commission (contract Bio-DNP 011721).

References

1 K. H. Hausser and D. Stehlik, *Adv. Magn. Reson.*, 1968, **3**, 79.
2 D. A. Hall, D. C. Maus, G. J. Gerfen, S. J. Inati, L. R. Becerra, F. W. Dahlquist and R. G. Griffin, *Science*, 1997, **276**, 930–932.
3 J.-H. Ardenkjaer-Larsen, B. Fridlund, A. Gram, L. Hansson, M. H. Lerche, R. Servin, M. Thaning and K. Golman, *Proc. Natl. Acad. Sci. U. S. A.*, 2003, **100**, 10158.
4 C.-G. Joo, K.-N. Hu, J. A. Bryant and R. G. Griffin, *J. Am. Chem. Soc.*, 2006, **128**, 9428.
5 V. S. Bajaj, M. L. Mak-Jurkauskas, M. Belenky, J. Herzfeld and R. G. Griffin, *Proc. Natl. Acad. Sci. U. S. A.*, 2009, **106**, 9244–9249.
6 T. Maly, G. T. Debelouchina, V. S. Bajaj, K.-N. Hu, C.-G. Joo, M. L. Mak-Jurkauskas, J. R. Sirigiri, P. C. A. Van der Wel, J. Herzfeld, R. J. Temkin and R. G. Griffin, *J. Chem. Phys.*, 2008, **128**, 052211.
7 P. Höfer, G. Parigi, C. Luchinat, P. Carl, G. Guthausen, M. Reese, T. Carlomagno, C. Griesinger and M. Bennati, *J. Am. Chem. Soc.*, 2008, **130**, 3254–3255.
8 M. J. Prandolini, V. P. Denysenkov, M. Gafurov, B. Endeward and T. F. Prisner, *J. Am. Chem. Soc.*, 2009, **131**, 6090–6092.
9 M. J. Prandolini, V. P. Denysenkov, M. Gafurov, S. Lyubenova, B. Endeward, M. Bennati and T. F. Prisner, *Appl. Magn. Reson.*, 2008, **34**, 399–407.
10 M. Reese, D. Lennartz, T. Marquardsen, P. Höfer, A. Tavernier, P. Carl, T. Schippmann, M. Bennati, T. Carlomagno, F. Engelke and C. Griesinger, *Appl. Magn. Reson.*, 2008, **34**, 301–311.
11 V. P. Denysenkov, M. J. Prandolini, A. Krahn, M. Gafurov, B. Endeward and T. F. Prisner, *Appl. Magn. Reson.*, 2008, **34**, 289–299.
12 M. Reese, M.-T. Tuerke, I. Tkach, G. Parigi, C. Luchinat, T. Marquardsen, A. Tavernier, P. Hofer, F. Engelke, C. Griesinger and M. Bennati, *J. Am. Chem. Soc.*, 2009, **131**, 15086–15087.
13 B. D. Armstrong and S. Han, *J. Chem. Phys.*, 2007, **127**, 104508–1-104508-10.
14 B. D. Armstrong and S. Han, *J. Am. Chem. Soc.*, 2009, **131**, 4641–4647.
15 B. D. Armstrong, P. Soto, J.-E. Shea and S. Han, *J. Magn. Reson.*, 2009, **200**, 137–141.
16 C. Luchinat and G. Parigi, *Appl. Magn. Reson.*, 2008, **34**, 379–392.
17 T. Nilsson, G. Parigi and J. Kowalewski, *J. Phys. Chem.*, 2002, **106**, 4476–4488.
18 J. Kowalewski, D. Kruk and G. Parigi, *Adv. Inorg. Chem.*, 2005, **57**, 41–104.
19 I. Bertini, C. Luchinat and G. Parigi, *Adv. Inorg. Chem.*, 2005, **57**, 105–172.
20 R. A. Wind and J.-H. Ardenkjaer-Larsen, *J. Magn. Reson.*, 1999, **141**, 347–354.
21 I. Solomon, *Phys. Rev.*, 1955, **99**, 559–565.
22 N. Bloembergen, *J. Chem. Phys.*, 1957, **27**, 572–573.
23 N. M. Loening, M. Rosay, V. Weis and R. G. Griffin, *J. Am. Chem. Soc.*, 2002, **124**, 8808–8809.
24 L. P. Hwang and J. H. Freed, *J. Chem. Phys.*, 1975, **63**, 4017–4025.
25 C. F. Polnaszek and R. G. Bryant, *J. Chem. Phys.*, 1984, **81**, 4038–4045.
26 Y. Ayant, E. Belorizky, P. H. Fries and J. Rosset, *J. Phys.*, 1977, **38**, 325–337.
27 H. F. Bennett, R. D. Brown III, S. H. Koenig and H. M. Swartz, *Magn. Reson. Med.*, 1987, **4**, 93–111.
28 G. Ferrante and S. Sykora, *Adv. Inorg. Chem.*, 2005, **57**, 405–470.
29 C. Luchinat and G. Parigi, *J. Am. Chem. Soc.*, 2007, **129**, 1055–1064.
30 D. Sezer, M. J. Prandolini and T. F. Prisner, *Phys. Chem. Chem. Phys.*, 2009, **11**, 6626–6637.

31 K. Yoshida, N. Matubayasi and M. Nakahara, *J. Chem. Phys.*, 2008, **129**, 214501–1-214501-9.
32 T. D. Davis, R. E. Christoffersen and G. M. Maggiora, *J. Am. Chem. Soc.*, 1975, **97**, 1347–1354.
33 R. O. C. Norman and B. C. Gilbert, *J. Phys. Chem.*, 1967, **71**, 14–19.
34 L. N. Ikryannikova, L. Y. Ustynyuk and A. N. Tikhonov, *J. Phys. Chem. A*, 2004, **108**, 4759–4768.
35 A. Abragam, *The Principles of Nuclear Magnetism*, Oxford University Press, Oxford, 1961.
36 B. H. Robinson, D. A. Haas and C. Mailer, *Science*, 1994, **263**, 490–493.
37 P. Höfer, P. Carl, G. Guthausen, T. F. Prisner, M. Reese, T. Carlomagno, C. Griesinger and M. Bennati, *Appl. Magn. Reson.*, 2008, **34**, 393–398.
38 D. Sezer, M. Gafurov, M. J. Prandolini, V. P. Denysenkov and T. F. Prisner, *Phys. Chem. Chem. Phys.*, 2009, **11**, 6638–6653.
39 M.-T. Türke, I. Tkach, M. Reese, P. Höfer and M. Bennati, *Phys. Chem. Chem. Phys.*, 2010, DOI: 10.1039/c002814m.

